QUASI-3D COUPLED ELECTRO-OPTICAL SIMULATION OF MQW AVALANCHE WAVEGUIDE PHOTODETECTORS

A. Nespola, M. Goano, G. Ghione, J. Haidar*

Dipartimento di Elettronica, Politecnico di Torino,
Corso Duca degli Abruzzi 24, 10129 Torino, Italy
E-mail: anespola@prometeo.polito.it
*ENSERG, Institut National Polytechnique de Grenoble
38016 Grenoble Cedex 1, France

ABSTRACT

The physics-based modeling of InAlAs/InGaAs waveguide MQW avalanche photodiodes is addressed through a coupled electro-optical quasi-3D approach, based on selfconsistent application of drift-diffusion simulation and the effective refractive index method. The application of the model to two recently proposed waveguide MQW APD structures shows a good agreement with experimental results.

INTRODUCTION

The huge progress made in digital optical fiber transmission systems call for high performance light detection devices. In the last decade, many efforts have been devoted to optimizing the existing structures and to devising quasi-ideal photodetectors. Multi-quantum well (MQW) and superlattice avalanche photodiodes (APD) based on InAlAs/InGaAs system have shown promising perfomances in terms of gain-bandwidth product, detectivity and noise factor [1]. More recently, it has been proposed [2–4] to couple MQW APDs to the waveguide photodetector concept, whereby the APD lighting is performed through an optical waveguide running orthogonal to the APD junction. This solution allows the separate optimization of optical and electrical performances, and improves the external quantum efficiency and the integrability of the device.

In the present work we address, through a quasi-3D approach, the physics-based coupled electro-optical simulation of two different waveguide MQW APDs. The first structure is a Separate Absorption and Multiplication (SAM) APD [2,3], while in the second one [4] the A and M regions coincide with the MQW. In both cases, the optical waveguide is modeled by means of the Effective Refractive Index (ERI) method, which provides the 3D modal field profiles and the modal propagation constants. According to the strength of the electro-optical coupling and to the structure length, the drift-diffusion electrical model of the APD can be 1D, 2D or 3D. In the recently proposed structures the optical field distribution is approximately uniform on the APD cross-section (for standard optical fiber excitation), so that a 2D analysis along the waveguide axis is adequate. Finally, for input power levels compatible with linear operation, the self-consistency of the electrical and optical models can be achieved iteratively, often in one iteration only. From the standpoint of the electrical performance evaluation, the model directly provides the output current (dark and under illumination). An estimate of the bandwidth and of the noise performances [5] can be derived from the electrical simulation by evaluating the delay component and the avalanche multiplication factor.

APD STRUCTURES

Due to the regenerative nature of the avalanche process, the gain-bandwidth product of APDs rises by increasing the ratio α/β between electron and hole ionisation coefficients [6]. Therefore an intrinsic MQW structure, based on the InAlAs/InGaAs system and first suggested by Capasso [7], has been used as multiplication zone in the photodiodes. The electrons captured into a quantum well after being accelerated by the electric field acquire an energy equal to the conduction band discontinuity ΔE_c. This results into a reduction of the threshold energy for the electron ionisation; hence the electron ionisation coefficient α increases, while β does not change appreciably. An electric field higher than about 10^5 V/cm induces a band bending such as to allow electrons to escape from the wells.

The schematic structure of the first avalanche waveguide photodetector that has been object of our study is shown in Fig. 1. The 40 μm long, 4 μm wide rectangular waveguide is fabricated by chemical etching of the

photodiode layers and by successive passivation with polymide. Hence, the waveguide and the photodiode have the same cross-section, which is shown in the left side of Fig. 1, where the MQW zone consists of nine pairs of alternating $In_{0.63}Ga_{0.37}As/In_{0.45}Al_{0.55}As$ layers. All the epitaxial layers are grown on an n-type InP substrate. An n-type 0.13 μm InGaAlAs second cladding layer, the undoped MQW region and a p-type 0.13 μm InGaAlAs second cladding layer are sandwiched between highly doped InAlAs cladding layers. A thin highly doped We denote this structure, where absorption and multiplication take place in the same MQW region, as W-APD. Since the light propagates along a direction normal to the flow of the photogenerated carriers, the thickness of the depletion region (and therefore the transit time τ_o) can be minimized without reducing the external quantum efficiency.

The performance of the W-APD is limited by the dark current, due to tunneling at the high electric fields required to achieve avalanche gain. This tunneling component can be eliminated with a structure providing separate regions for multiplication and absorption (SAM-APD [8], see Fig. 1, right). The SAM-APD structure investigated in the present work has a wider waveguide in order to improve the coupling between the gaussian field emitted by a single-mode fiber and the guided optical field. An optimized SAM-APD ensures that the electric field in the MQW multiplication layers is high enough to provide high avalanche gain, while in the $In_{0.53}Ga_{0.47}As$ absorbing layer the electric field is kept below the threshold where tunneling becomes significant.

APD MODELS

The photodiode model couples an optical model for the waveguide to a physics-based model for the electronic transport.

The ERI and transverse resonance methods are employed to handle the multi-layer waveguide structures [9]. This approach provides the waveguide modes and the 3D optical field profile. The light absorption occurring in the absorption region of the APD is taken into account through its contribution to the imaginary part of the refractive indices. The transverse structure is multi-modal along the lateral direction (y axis) only; Fig. 2 provides an example of the optical field pattern for the fundamental mode in SAM-APDs. The coupling between the gaussian field emitted by a single-mode fiber and the TE_{00} mode is more than one order of magnitude stronger than the coupling with the TE_{02} mode, thus making the excitation of higher-order modes almost negligible in both structures.

From the optical field and power profile, the distributions of generated electron-hole pairs and the total current flowing through the photodiode can be estimated. The drift-diffusion model used in the electrical simulation includes Shockley-Read-Hall and thermal generation-recombination processes, avalanche multiplication and band-to-band tunneling. The MQW has been described as an homogeneous region whose parameters depend on the depth, width and distance of the wells. To simulate the avalanche multiplication, the electric field dependence of the ionisation coefficients α and β has been taken into accont through the following model [10]:

$$\alpha = A_\alpha \cdot e^{-\frac{b_\alpha}{E}} \quad (1)$$

$$\beta = A_\beta \cdot e^{-\frac{b_\beta}{E}} \quad (2)$$

The coefficients A and b were estimated from experimental results for an InAlAs/InGaAs MQW [4].

The band profile across the junction in reverse bias for the SAM-APD is shown in Fig. 3. One can easily identify the high-field multiplication region and the low-field absorption region (between 0.5 and 1 μm approximately). For reverse bias lower than a "blocking voltage" around -10 V, the photogenerated carriers are confined in the absorption region and do not undergo multiplication, so that the SAM-APD is virtually inactive.

The Teich approach [5] has been exploited to simply relate the excess avalanche noise factor F and the multiplication factor M.

RESULTS

The two APD structures previously discussed were manufactured and measured in the CNET laboratories at Bagneux (France), within the framework of a laurea/DEA work at Politecnico di Torino and Institut National Polytechnique de Grenoble [11].

The simulated and measured dark currents of W-APD are shown in Fig. 4. For bias voltages below 3 V the dark current is negligible and is mainly due to the generation-recombination and diffusion current. For bias voltages around $5 \div 6$ V the tunneling effect comes into play producing dark currents of a few μA and giving rise to the complex behaviour shown, which is in reasonable agreement with the experiments. Comparing these

results with the dark current of SAM-APDs (Fig. 5), we immediately recognize the advantages of a structure where absorption and multiplication regions are separated: in the SAM-APD, the contribution of tunneling to the dark current exceeds the generation-recombination component only at bias voltages above 15 V. The "blocking voltage" effect previously discussed for SAM-APDs may be clearly observed in Fig. 5, which presents the simulated and measured currents under illumination for an incident power $P = -40\,\text{dBm}$ and an optical wavelength $\lambda = 1,55\,\mu\text{m}$.

The frequency response of a SAM-APD with an absorption region of $0.2\,\mu\text{m}$ has been characterized by means of the optical heterodyne method [12]. The measurement system consists of two tunable lasers at $1.55\,\mu\text{m}$ whose frequency difference may be tuned over $0 \div 40\,\text{GHz}$ [11]. The optical signals are combined by a 3 dB coupler and sent to the photodiode through a single-mode fiber. The microwave signal generated in the photodiode by optical mixing is collected at the output by a high frequency probe and is sent to an HP 8564E spectrum analyzer. The calibrated frequency response is shown in Fig. 6. A maximum 3 dB-bandwidth of 21.5 GHz is achieved for a bias voltage of 20 V. The 3 dB-bandwidth decreases as the reverse voltage is increased, because of the rise of the multiplication factor and, consequently, of the effective transit time. The bandwidth degradation as a function of the multiplication factor is shown in Fig. 7.

Noise measures are essential to calculate the multiplication factor and the ensuing gain-bandwidth product. In order to measure the white noise at frequencies where $1/f$ and generation-recombination noise are neglegible, it is necessary to work at about 10 MHz. The noise spectral density of the photodiode is obtained by sending to the device a non-modulated optical signal and by reading the corresponding output with a spectrum analyser. The comparison between the noise spectral density of the SAM-APD, measured at different values of the photocurrent I_{ph}, and the theoretical noise spectral density of a PIN detector ($2qI_{ph}$), allows the evaluation of the excess noise factor and of the multiplication factor (see Fig. 8).

CONCLUSIONS

The performances of two types of edge-coupled waveguide APDs based on a InAlAs/InGaAs MQW structure have been simulated with a selfconsistent electro-optical quasi-3D model. The theoretical results have been compared with measurements made at CNET laboratories, and are in good agreement with experiments for both structures. In particular, a satisfactory description of the tunneling effects in the SAM APD device has been demonstrated.

References

[1] B. F. Levine, "Quantum-well infrared photodetectors," *J. Appl. Phys.*, vol. 74, no. 8, pp. R1–R81, Oct. 1993.

[2] M. Shishikura, H. Nakamura, S. Hanatani, S. Tanaka, T. Miyazaki, and S. Tsuji, "A InAlAs/InGaAs superlattice avalanche photodiode with a waveguide structure," in *Fifth Optoelectronics Conference (OEC '94) Technical Digest*, Makuhari Messe, July 1994, pp. 67–70.

[3] M. Shishikura, H. Nakamura, S. Hanatani, S. Tanaka, H. Sano, and S. Tsuji, "A waveguide InAlAs/InGaAs superlattice avalanche photodiode with a 120-GHz gain-bandwidth product," in *IPR. Topical Meeting on Integrated Photonics Research*, Diana Point, CA, Feb. 1995, pp. 9–11.

[4] S. Hanatani, M. Shishikura, S. Tanaka, H. Kitano, T. Miyazaki, and H. Nakamura, "A strained InAlAs/InGaAs superlattice avalanche photodiode for operation at an IC-power-supply voltage," in *IPRM 95. Seventh International Conference on Indium Phosphide and Related Materials*, Sapporo, May 1995, pp. 369–372.

[5] M. C. Teich, K. Matsuo, and B. E. A. Saleh, "Excess noise factor for conventional and superlattice avalanche photodiodes and photomultiplier tubes," *IEEE J. Quantum Electron.*, vol. QE-22, no. 8, pp. 1184–1193, Aug. 1986.

[6] S. R. Forrest, "Gain-bandwidth-limited response in long-wavelength avalanche photodiodes," *J. Lightwave Technol.*, vol. LT-2, no. 1, pp. 34–39, Feb. 1984.

[7] F. Capasso, J. Allam, A. Y. Cho, K. Mohammed, R. J. Malik, A. L. Hutchinson, and D. Sivco, "New avalanche multiplication phenomenon in quantum well superlattices: Evidence of impact ionization across the band-edge discontinuity," *Appl. Phys. Lett.*, vol. 48, no. 19, pp. 1294–1296, May 1986.

[8] J. C. Campbell, W. S. Holden, G. J. Qua, and A. G. Dentai, "Frequency response of InP/InGaAsP/InGaAs avalanche photodiode with separate absorption "grading" and multiplication regions," *IEEE J. Quantum Electron.*, vol. QE-21, no. 11, pp. 1743–1746, Nov. 1985.

[9] E. Marantonio, R. E. Zich, and I. Montrosset, "Alternative expression of the dispersion equation in multilayered structures," *IEE Proc.-J*, vol. 137, no. 6, pp. 357–360, Dec. 1990.

[10] G. E. Stillman and C. M. Wolfe, "Avalanche photodiodes," in *Infrared Detectors II*, R. K. Willardson and A. C. Beer, Eds., vol. 12 of *Semiconductors and Semimetals*, pp. 291–393. Academic Press, New York, 1977.

[11] A. Bonzo, "Simulazione e caratterizzazione di fotorivelatori a valanga MQW a guidaggio ottico," M.S. thesis, Politecnico di Torino, Oct. 1996.

[12] R. T. Hawkins II, M. D. Jones, S. H. Pepper, and J. H. Goll, "Comparison of fast photodetector response measurements by optical heterodyne and pulse response techniques," *J. Lightwave Technol.*, vol. LT-9, no. 10, pp. 1289–1294, Oct. 1991.

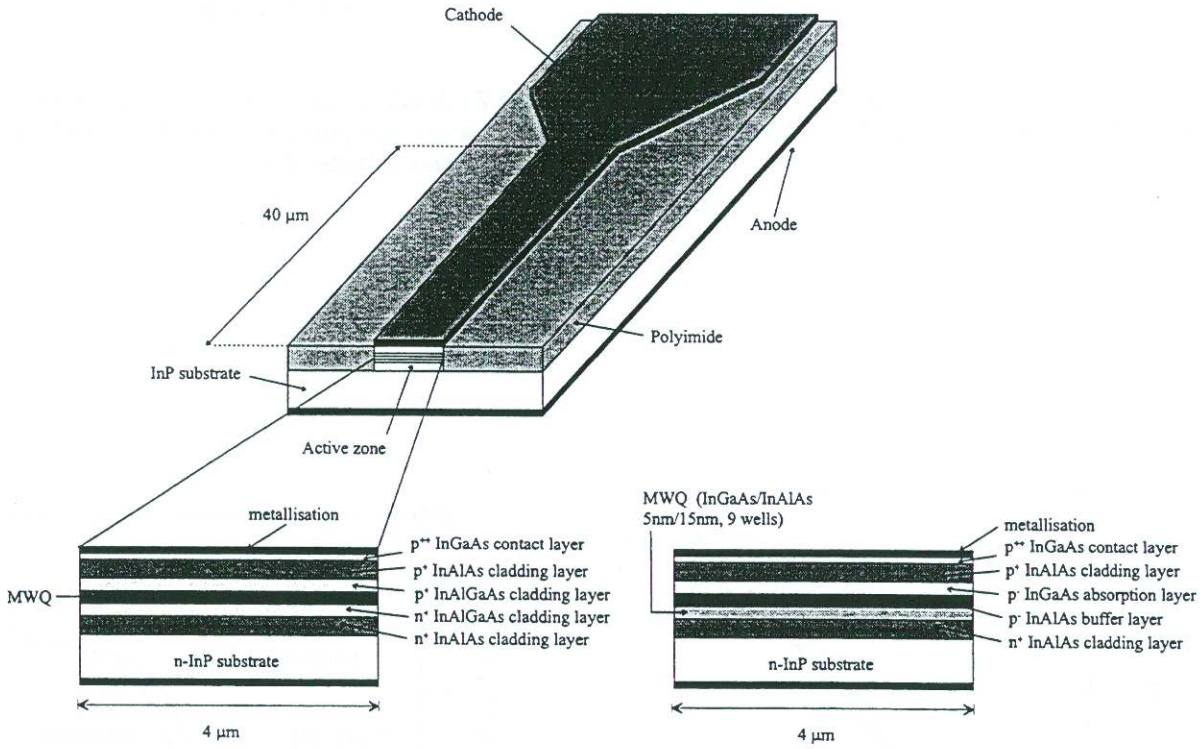

Figure 1: Left: structure and cross-section of the waveguide MQW APD. Right: cross-section of the MQW SAM-APD.

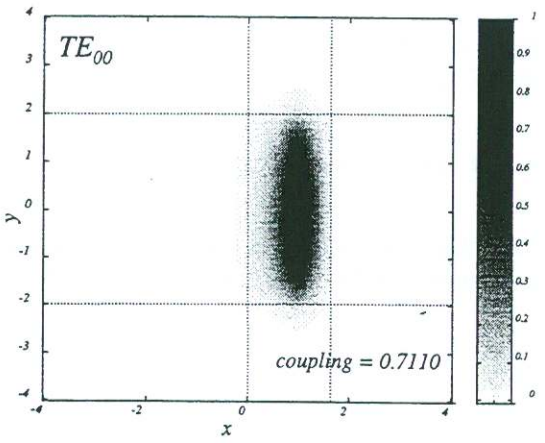

Figure 2: Cross-section map of the fundamental mode (TE_{00}) in the SAM-APD structure.

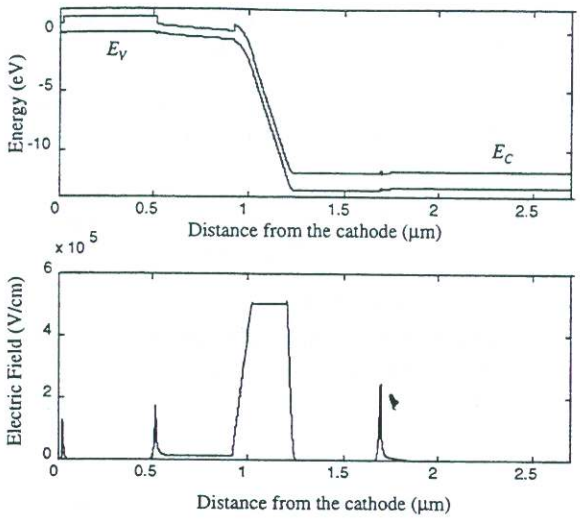

Figure 3: Band diagram (above) and electric field (below) across the junction in the SAM-APD structure for a bias voltage of −12 V.

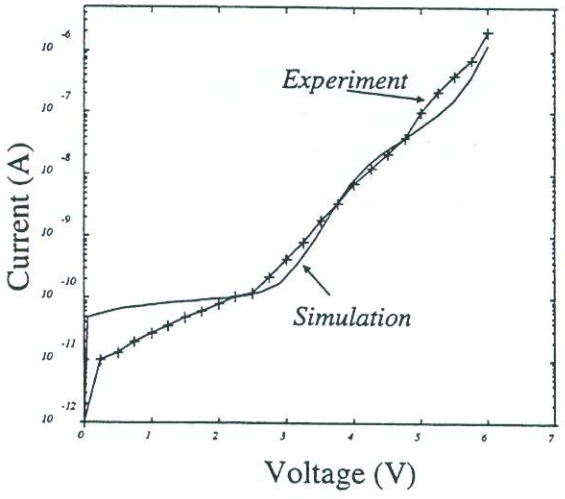

Figure 4: W-APD: dark current.

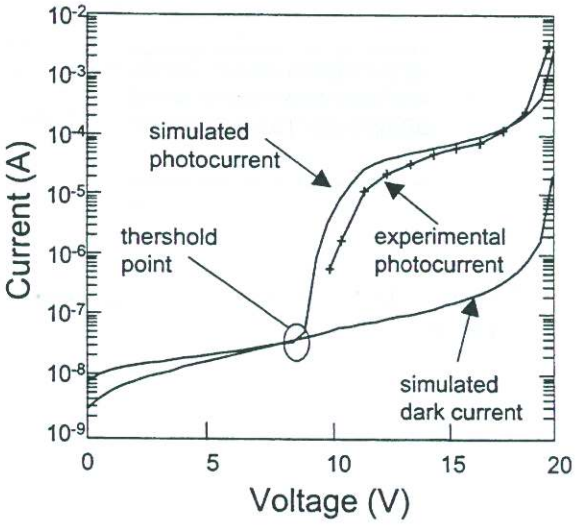

Figure 5: SAM-APD: photocurrent and dark current.

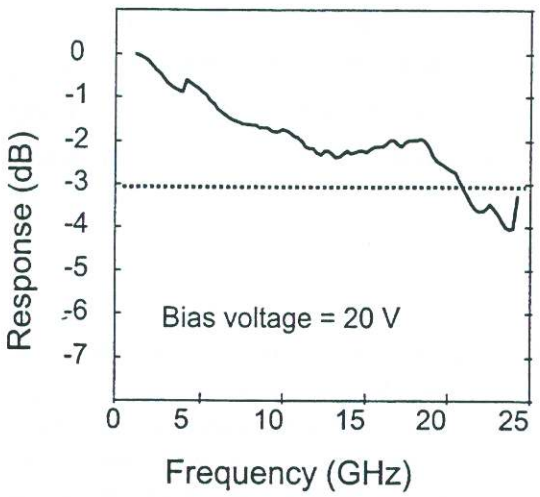

Figure 6: SAM-APD: frequency response.

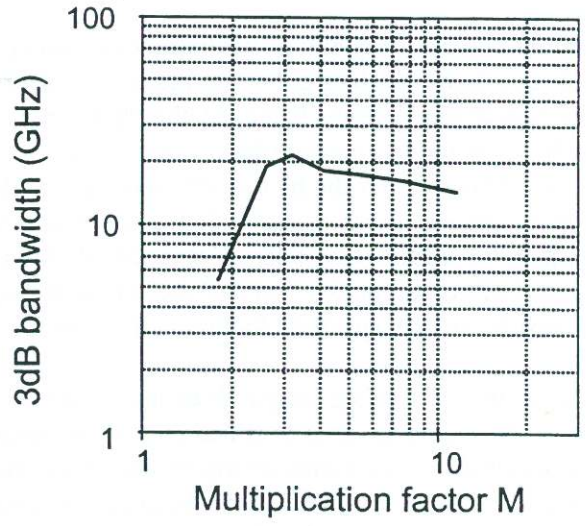

Figure 7: SAM-APD: theoretical 3 dB-bandwidth vs. multiplication factor.

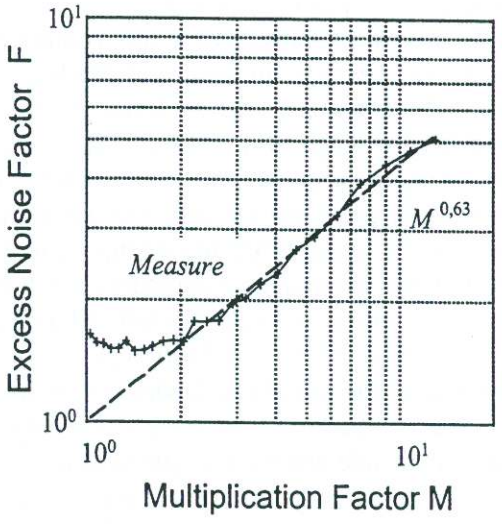

Figure 8: SAM-APD: experimental values of excess noise factor and comparison with the theoretical values of a PIN detector.